

# Pyridyl-Decorated Self-Folding Heptaamide Cavitanths as Ligands in the Rhodium-Catalyzed Hydrogenation of Norbornadiene

Saša Korom<sup>[a]</sup> and Pablo Ballester\*<sup>[a,b]</sup>

**Keywords:** Cavitanths / Homogeneous catalysis / Hydrogenation / Rhodium

The different binding geometries exhibited in solution by the Rh<sup>I</sup> cationic complexes of three regioisomeric self-folding heptaamide cavitanths, each decorated with one pyridyl group at the upper rim, are taken into account to explain the

diverse distributions of products obtained when these complexes are employed as catalysts for the hydrogenation of norbornadiene.

## Introduction

The application of supramolecular concepts to catalysis is targeted through different approaches.<sup>[1–7]</sup> Among them, the encapsulation of catalytic metal centers within molecular assemblies has proven to be highly efficient.<sup>[8–10]</sup> By this approach, the stability,<sup>[11,12]</sup> reactivity,<sup>[13]</sup> and selectivity<sup>[11,14,15]</sup> normally observed for the catalytic metal center free in solution can be radically altered and modified.

Encapsulation of a catalytic metal center has been achieved successfully through ligand-template directed assembly of the container.<sup>[16–18]</sup> Alternatively, an organometallic complex can be used in the form of a guest in a molecular or supramolecular container.<sup>[19]</sup> In the latter case, the molecular vessel acts as a second coordination sphere ligand. Recently, one of us<sup>[11]</sup> reported that self-folding octaamide cavitant **1**<sup>[20,21]</sup> (Figure 1), based on a resorcin[4]arene scaffold, binds the organometallic complex [Rh(NBD)<sub>2</sub>·BF<sub>4</sub> (3·BF<sub>4</sub>) with high affinity in dichloromethane solution. The binding process mainly produces a 1:1 inclusion complex 3<sup>+</sup>⊂**1**. The inclusion process, however, also induces the partial dissociation of one of the NBD ligands of 3<sup>+</sup>, affording a small quantity of another inclusion complex – (NBD)Rh<sup>+</sup>⊂**1**.

Interestingly, the mixture of the two inclusion cationic Rh<sup>I</sup> complexes was found to be catalytically competent in the hydrogenation of NBD. When the hydrogenation is performed on a laboratory scale, with the supramolecular system **1** (1.2 mol-%) and 3<sup>+</sup> (1.0 mol-%), the GC/FID analysis of the crude product reveals that it is composed of nor-

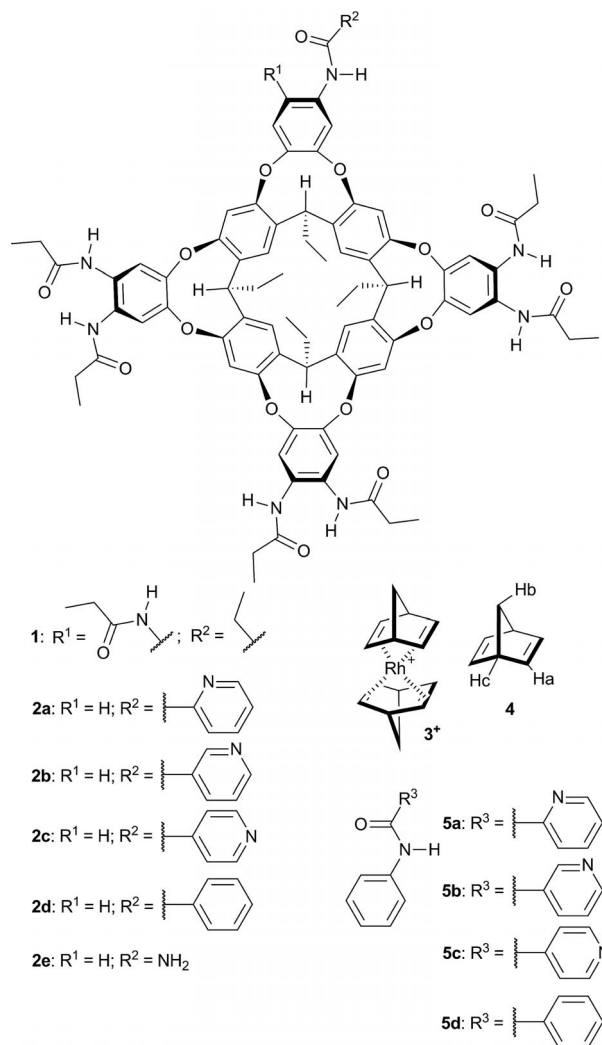


Figure 1. Molecular structures of the self-folding cavitanths octaamide **1** and heptaamides **2a–d**, together with the cationic Rh<sup>I</sup> complex **3<sup>+</sup>**, norbornadiene (NBD, **4**), and the monoamides **5a–d** used as model systems.

[a] Institute of Chemical Research of Catalonia (ICIQ), Av. Països Catalans 16, 43007 Tarragona, Spain  
E-mail: pballester@iciq.es  
<http://www.iciq.es/porta1/325/default.aspx>

[b] Catalan Institution for Research and Advanced Studies (ICREA)

Pg. Lluís Companys 23, 08010 Barcelona, Spain

Supporting information for this article is available on the WWW under <http://dx.doi.org/10.1002/ejoc.201402385>.

bornene (**6**, 72%), nortricyclene (**7**, 3.7%), and dimer **8** (24.2%, Figure 2). This finding constitutes a remarkable result because the hydrogenation of NBD promoted by  $3^+$  alone (1 mol-%) produces almost exclusively dimer **8** as the result of the known reductive NBD dimerization.<sup>[22]</sup> We hypothesized that the dimer **8** also detected in the NBD catalytic hydrogenation in the presence of the mixture of inclusion complexes  $3^+ \cdot \mathbf{1}$  and (NBD)Rh<sup>+</sup>·**1** must be produced by the presence of a small quantity of  $3^+$  that is released into the solution during hydrogenation.

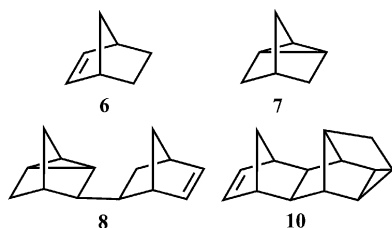


Figure 2. Line drawing structures of norbornene (**6**), nortricyclene (**7**), dimer **8**, and dimer **10**.

Here we disclose the synthesis of a series of regioisomeric heptaamide self-folding cavitands **2a–c**, which are structurally related to **1** but each possess a single pyridyl residue installed at the upper rim.

In addition, we report the results obtained for the Rh<sup>I</sup>-catalyzed hydrogenation of NBD in the presence of these heptaamide cavitands **2** as ligands. The design of the unimolecular pyridyl containers **2** for the inclusion of the Rh<sup>I</sup> metal center is based on the combination of two supramolecular strategies: (a) ligand-templated assembly, and (b) use of an organometallic cationic complex as the guest in the molecular container. Our expectations were that the pyridyl residue would be able to act in a cooperative manner with the electron-rich interior of the cavitand (cation- $\pi$ ), thus increasing the thermodynamic stabilities of the Rh<sup>I</sup> cavitplexes derived from **2** relative to the previously reported system based on the unfunctionalized octaamide cavitand **1**. If this were the case, the release of  $3^+$  or (NBD)Rh<sup>+</sup> complexes in solution during the hydrogenation should be reduced, and the formation of dimer **8** might even be eliminated.

## Results and Discussion

### Synthesis of the Cavitands and Assignment of Conformation

The regioisomeric pyridyl cavitands **2a–c** and the phenyl heptaamide cavitand **2d** were prepared by acylation of the known monoamino hexaamide cavitand **2e**<sup>[23]</sup> with the corresponding acylpyridyl or benzoyl chlorides, respectively. We used Schotten–Baumann conditions to perform the reactions. The yields ranged from 70–85%. Cavitand **2d**, with a phenyl group instead of a pyridyl residue, was prepared as a reference model system. By analogous synthetic procedures, a series of *N*-phenylpyridinecarboxamides **5a–c**

and *N*-phenylbenzamide (**5d**) were produced as additional reference systems (see Figure 1 for structures).

The X-ray structures of cavitands **2a**, **2b**, and **2d** revealed that they each adopted the vase conformation in the solid state. This conformation is stabilized by the formation of an array of six intramolecular hydrogen bonds between the amide functions at the upper rim.<sup>[20]</sup> In the cases of **2a** and **2b**, one molecule of the crystallization solvent is included in the aromatic cavity. It is worth noting that cavitands **2** are chiral molecules possessing two elements of asymmetry. The nonsymmetric substitution of one of the four phenyldioxo bridges creates asymmetry in the covalent structure of a cavitand **2**, resulting in chiral stereogenic carbon atoms (Figure 3 side views). In this sense, enantiomers of **2** can easily be differentiated by the reverse absolute configurations of the methine carbon atom (*R* or *S*) embedded in the nine-membered ring encompassing the phenyldioxo bridge with the single amide.

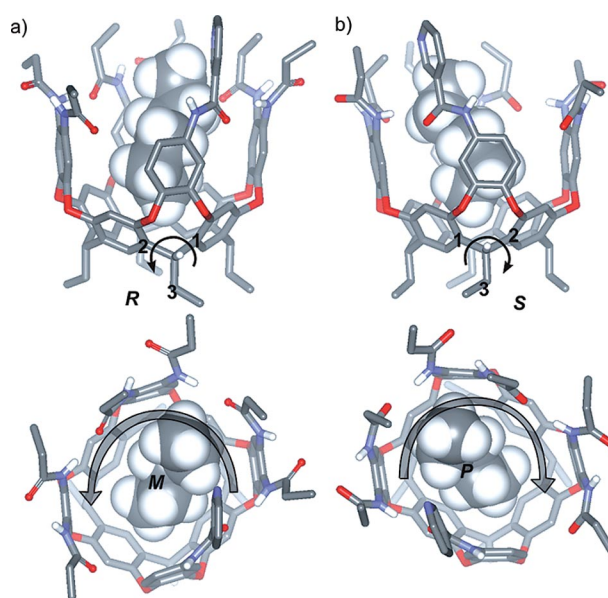


Figure 3. Side and top views of the X-ray structures of the racemic pair of diastereoisomers present in the crystal packing of **2b**: (a) (*M,R*)-**2b** and (b) (*P,S*)-**2b**. Nonpolar hydrogen atoms of **2b** have been omitted for clarity. The included hexane (from the solvent) molecule is shown as a CPK model.

The other element of asymmetry is of supramolecular origin.<sup>[24]</sup> It originates from the unidirectional orientation of the carbonyl groups of the amides at the upper rim (Figure 3, top views). The amides' directionality derives from the formation of an intramolecular belt of hydrogen bonds.<sup>[25]</sup> Because of this second element of asymmetry, cavitands **2** can exist as mixtures of two diastereoisomeric pairs of mutual enantiomers (four diastereomers).

Interestingly, only one of two possible racemic pairs is detected in the packings of single crystals obtained for **2b** and **2d** [(*M,R*)-**2** and (*P,S*)-**2**]. The preferred sense of orientation (*P/M*) of the belt of hydrogen-bonded amides is controlled by the favoured role of the single amide as hydrogen-bond acceptor.

In the particular case of **2a**, the crystal packing shows that the aromatic cavity is filled with one acetone molecule and also with the ethyl group of an adjacent cavitaand molecule, forming a dimeric aggregate (Figure 4).

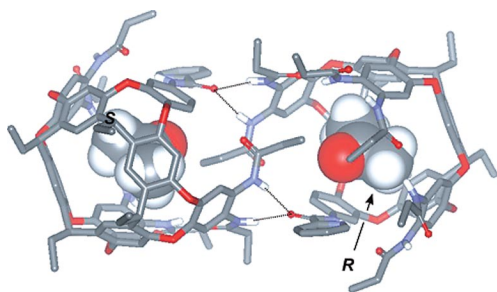


Figure 4. Solid-state structure of the dimer of **2a**. Bifurcated hydrogen bonds are depicted as dotted lines. The molecule of acetone (from the solvent) included in **2a** is shown as a CPK model. Non-polar hydrogen atoms in **2a** have been omitted for clarity.

The dimer is held together by four bifurcated intermolecular hydrogen bonds established between the carbonyl oxygen atom of the single-amide group of each monomer and the NH groups of two amide groups of the adjacent **2a** molecule. The intermolecular interactions disrupt the unidirectional orientation of the amide groups at the upper rim of **2a**. Two enantiomers of **2a** are present in each dimer.

The  $^1\text{H}$  NMR spectra of  $\text{CD}_2\text{Cl}_2$  solutions of cavitaands **2a–d** each feature a single set of proton signals consistent with  $C_1$  symmetry. The signals of the amide protons are downfield-shifted, suggesting their involvement in hydrogen bonding. The four chemically non-equivalent methine protons resonate at  $\delta \approx 5.6$  ppm. Taken together, these results suggest that cavitaands **2** exist as enantiomeric pairs of single diastereoisomers in solution, adopting the vase conformation.<sup>[26]</sup> These results are in agreement with the solid-state data and with reported findings for related heptaamide cavitaands.<sup>[23]</sup>

### Binding Studies of Cavitaands **2** and Model Systems **5** with $3\text{-BF}_4$

Simple molecular modeling studies suggested two different geometries (*endo* and *exo*) for the coordination complexes formed through the interaction of the pyridyl nitrogen atom in **2a** and **2b** and the rhodium metal of (NBD)  $\text{Rh}^+$ . The formation of the N–Rh bond induces the dissociation of one NBD ligand in  $3^+$  (vide infra). In the *exo* binding geometry the (NBD) $\text{Rh}^+$  unit would point away from the aromatic cavity (Figure 5, d).

Conversely, in the *endo* conformer the (NBD) $\text{Rh}^+$  unit is directed towards the aromatic cavity (Figure 5, c). Compound **2c**, with the nitrogen atom in the *para* position of the pyridyl substituent, would be expected to direct the (NBD) $\text{Rh}^+$  unit away from the aromatic cavity in any of its conformers.

For the three pyridyl cavitaands **2a–c**, owing to the weak coordination interaction that exists between  $\text{Rh}^I$  and nitrogen atoms,<sup>[27]</sup> it is sensible to consider the direct inclusion

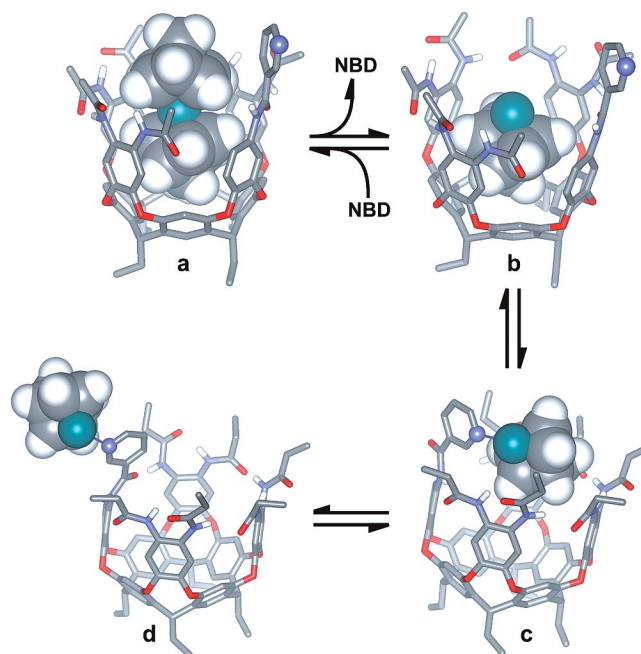


Figure 5. Energy-minimized structures of the different metallo complexes resulting from the interaction of **2b** with  $3^+$ : (a)  $3^+ \subset \mathbf{2b}$ , (b) (NBD) $\text{Rh}^+ \subset \mathbf{2b}$ , (c) *endo*-(NBD) $\text{Rh}^+ \cdot \mathbf{2b}$ , and (d) *exo*-(NBD) $\text{Rh}^+ \cdot \mathbf{2b}$ . The  $\text{Rh}^I$  metal and the NBD ligands are shown as CPK models; **2b** is displayed in stick representation. The nitrogen atom of the pyridyl residue is highlighted as a larger ball. Non-polar hydrogen atoms in **2b** have been omitted for clarity.

of  $3^+$  (Figure 5, a) or (NBD) $\text{Rh}^+$  (Figure 5, b) in their aromatic cavities without assistance of the coordination bond with the pyridyl nitrogen atom.

The calculated energies (MM3 as implemented in SCIGRESS v3.0) for the complexes of **2a/2b** with (NBD) $\text{Rh}^+$  in *exo* and *endo* coordination geometries indicate that the former is energetically preferred for complex (NBD) $\text{Rh}^+ \cdot \mathbf{2a}$  whereas the latter is favored in the case of (NBD) $\text{Rh}^+ \cdot \mathbf{2b}$ .

Because the *endo*-(NBD) $\text{Rh}^+ \cdot \mathbf{2b}$  complex features a cooperative binding mode, which combines the formation of a coordination N– $\text{Rh}^I$  bond with cation– $\pi$  interactions, we expected that its thermodynamic and kinetic properties would be improved in relation to those of **2a** or the parent  $3^+ \subset \mathbf{1}$  complex. This improvement should translate into reduced leaking of (NBD) $\text{Rh}^+$  into the bulk solution under hydrogenation conditions. A recent computational study showed that the reductive dimerization of NBD to afford dimer **8** requires the coordination of three NBD molecules to the  $\text{Rh}^I$  center.<sup>[28]</sup> For steric reasons, three molecules of NBD cannot coordinate simultaneously to  $\text{Rh}^I$  if the metal center is included in the cavity of **1** or **2**. In short, cavitaand **2b** stands out as an ideal candidate to suppress the formation of dimer **8** observed in the rhodium-catalyzed hydrogenation of NBD.

With the aim of studying the binding properties (towards  $3^+$ ) of the pyridyl carboxamide residues installed at the upper rim of each of cavitaands **2a–c** in isolation from those of the close-by aromatic cavity, we synthesized pyridyl carboxamides **5a–d** as model systems and studied their binding

properties. The interactions between **5a–d** and **3**·BF<sub>4</sub> were probed by <sup>1</sup>H NMR spectroscopy. The addition of 0.8 equiv. of **3**·BF<sub>4</sub> to separate dichloromethane solutions of the three pyridine carboxamides **5a–c** (4.5 mM) induced significant changes in the chemical shifts of the signals of the amide NH and pyridyl protons relative to those in the free ligands. The results of the titration experiments indicate that the coordination of carboxamides **5a–c** to **3**<sup>+</sup> induces different levels of dissociation of one of the NBD ligands, yielding free NBD and the 1:1 heteroleptic complexes **5a–c**·Rh(NBD)<sup>+</sup>. The complexes are each stabilized by the formation of a N–Rh<sup>I</sup> coordination bond. The protons of the free and bound NBDs are observed as separate signals, indicating that they are involved in a chemical exchange process that is slow on the NMR timescale. Conversely, a single set of proton signals is observed for each of the *N*-phenyl carboxamides **5a–c**. Moreover, the extents to which the 1:1 complexes **5a–c**·Rh(NBD)<sup>+</sup> are formed in equimolar solutions depend on the position of the nitrogen atom in the pyridyl substituent of the ligand. In the case of **5a**, in which the pyridyl nitrogen atom is *ortho* to the amide function, the complex **5a**·Rh(NBD)<sup>+</sup> is formed quantitatively in an equimolar mixture of partners. Most likely, this is due to the existence of a ditopic interaction between the ligand **5a** and the Rh<sup>I</sup> metal center. Additional evidence for Rh<sup>I</sup> coordination to the carbonyl oxygen in **5a**·Rh(NBD)<sup>+</sup> was provided by the downfield shift experienced by the amide NH. In striking contrast, ligand **5d**, lacking the pyridyl residue, induces the dissociation of **3**<sup>+</sup> into NBD and the formation of **5d**·Rh(NBD)<sup>+</sup> to a minimum extent. Therefore, ligand **5d** must coordinate to the Rh<sup>I</sup> through its carbonyl oxygen atom. It is worth mentioning that in this latter case the chemical exchange processes both of free and bound NBD and of free and bound ligand **5d** are slow on the NMR timescale.

Next, we investigated the binding properties of the cavitand series **2** towards **3**<sup>+</sup>. Using 1D and 2D <sup>1</sup>H NMR spectroscopy, we analyzed the compositions of separate CD<sub>2</sub>Cl<sub>2</sub> solutions containing 1 equiv. of **3**<sup>+</sup> and 1.2 equiv. of each cavitand **2a–d**. In all cases, the proton signals corresponding to the free NBD (**4**) were easily identified (H<sub>a</sub>, H<sub>b</sub>, and H<sub>c</sub>; see the Supporting Information). This observation parallels the findings made with the model systems **5a–c**. In short, the coordination of the pyridyl substituents in cavitands **2a–c** with **3**<sup>+</sup> induces the dissociation of one of their NBD ligands to different extents. The presence of cross-peaks in 2D EXSY experiments revealed that the protons of free NBD were involved in chemical exchange processes with bound NBD molecules in more than one magnetic environment. The olefinic proton (H<sub>a</sub>) of the free NBD was the best signal to analyze the multi-site exchange systems. In the case of **2a** (2-carboxypyridine cavitand) interacting with **3**<sup>+</sup>, 1 equiv. of the free NBD is released and found to exchange with NBD units in two different bound states. The quantitative dissociation of **3**<sup>+</sup> is in agreement with the result obtained for the model **5a**. Most likely, the ditopic (N,O) metal-ligand interaction present in the **2a**·Rh(NBD)<sup>+</sup> complex is responsible for its high thermodynamic stability. On the basis of the molecular modeling studies

discussed above, we assigned *endo* and *exo* geometries to the two coordination complexes of **2a**·Rh(NBD)<sup>+</sup>. The two complexes are engaged in a chemical exchange process. The complexes' interconversion is slow on the NMR timescale because it must occur through a sizeable conformational change of the cavitand (vase-to-kite) rather than a simple C–C bond rotation. The small integral measured for the signal that resonates furthest upfield ( $\delta = -2.64$  ppm) and is assigned to the H<sub>c</sub> protons of the Rh(NBD)<sup>+</sup> included in the aromatic cavity of **2a** indicates that the *exo* conformer is the major species (>90%) in solution.

The use of cavitand **2b** (3-carboxypyridine) produced a more complex distribution of species. From the integrals of selected proton signals, we calculated the percentages of the different species in solution to be: 62% of the *exo*-**2b**·Rh(NBD)<sup>+</sup> conformer, 21% of the *endo*-**2b**·Rh(NBD)<sup>+</sup> conformer, and 17% of the inclusion complex **3**<sup>+</sup>·**2b** not assisted by the formation of a coordination bond. Contrary to our expectations, the *endo*-**2b**·Rh(NBD)<sup>+</sup> complex is not the major species in solution. Interestingly, the protons of the bound NBD in *endo*-**2b**·Rh(NBD)<sup>+</sup> resonate as diastereotopic signals, due to cavity's chirality imparted by the unidirectional orientation of the amide groups at the upper rim. By using competitive pairwise experiments we also determined that the complexes of cavitand **2b** had a minimal thermodynamic advantage with respect to **3**<sup>+</sup>·**1**. This result was again completely unexpected on the basis of our initial hypothesis.

The third pyridyl cavitand **2c** (4-carboxypyridine), with its N atom pointing away from the aromatic cavity, produced a very different distribution of complexes. The major species detected in solution is the inclusion complex (NBD)Rh<sup>+</sup>·**2c** (68%), which does not involve a coordination bond, probably due to geometric constraints. The coordination complex **2c**·Rh(NBD)<sup>+</sup> (23%) and the inclusion complex **3**<sup>+</sup>·**2c** (9%) are also present in the mixture. The protons of the external NBD ligands in the last complex also resonate as diastereotopic signals.

Finally, cavitand **2d** (carboxyphenyl) produced the inclusion complexes (NBD)Rh<sup>+</sup>·**2d** (50%) and **3**<sup>+</sup>·**2d** (45%) in similar quantities, with a small amount of free **3**<sup>+</sup> (5%) remaining in solution.

### Rhodium-Catalyzed Hydrogenations of NBD with the Model Systems and the Cavitands as Ligands

The coordination complexes of **5a–d** and **3**·BF<sub>4</sub> were tested as catalysts in the hydrogenation of norbornadiene **4** (1 mol-% of **3**·BF<sub>4</sub>, 1.2 mol-% of **5a–d**, room temp., 1 atm H<sub>2</sub>). The GC/FID analysis of the hydrogenation crude products after 45 min reaction time showed significant differences in composition. The results obtained are summarized in Table 1.

Several conclusions can be drawn from the data: (1) the monotopic coordination of the Rh<sup>I</sup> metal center to the pyridyl nitrogen atom in ligands **5b** and **5c** produces highly active species for the hydrogenation of NBD that exclusively

Table 1. Percentages of NBD (**4**) consumed (“con”) after 45 min reaction time and the resulting product distributions (%) for the laboratory-scale catalytic hydrogenations performed in this study (see the Supporting Information for experimental details).

Entry	System	% <b>4</b> con	Product distribution in % <sup>[a]</sup>				
			<b>6</b>	<b>7</b>	<b>8</b>	<b>10</b>	other
1	<b>3</b> <sup>[b]</sup>	80	0.9	1.0	73.4	24.7	0
2	<b>3</b> <sup>[c]</sup>	30	2.9	0	0	92.2	4.9
3	<b>1</b> + <b>3</b> <sup>+</sup>	55	81.7	0.7	15.6	2.0	0
4	<b>2a</b> + <b>3</b> <sup>+</sup>	30	60.1	39.9	0	0	0
5	<b>5a</b> + <b>3</b> <sup>+</sup>	35	47.6	52.4	0	0	0
6	<b>2b</b> + <b>3</b> <sup>+</sup>	35	42.4	57.6	0	0	0
7	<b>5b</b> + <b>3</b> <sup>+</sup>	30	0	100	0	0	0
8	<b>2c</b> + <b>3</b> <sup>+</sup>	60	18.3	81.7	0	0	0
9	<b>5c</b> + <b>3</b> <sup>+</sup>	50	0	100	0	0	0
10	<b>2d</b> + <b>3</b> <sup>+</sup>	60	64.6	0	35.4	0	0
11	<b>5d</b> + <b>3</b> <sup>+</sup>	75	1.1	1.3	72.9	23.5	1.2

[a] Values (%) are corrected under the assumption that the response factor of the dimer is twice that of the monomer. [b] Without pre-activation of catalyst. [c] No hydrogen.

yield nortricyclene (**7**, Entries 7 and 9), (2) the ditopic N,O coordination of the Rh<sup>I</sup> center exerted by ligand **5a** hydrogenates NBD to produce a close to 50:50 mixture of norbornene (**6**) and nortricyclene (**7**, Entry 5), and (3) ligand **5d**, lacking the pyridyl group, does not have a significant effect on the catalytic properties exhibited by **3**<sup>+</sup> alone (Entries 1 and 11).

It is worth noting that dimer **10** is produced in significant amounts in Entries 1 and 11. On the other hand, catalyst **3**<sup>+</sup> in the absence of H<sub>2</sub> induces the dimerization of NBD to yield dimer **10** (Entry 2).<sup>[29]</sup>

We learned during the course of this study that the reaction conditions used to perform the hydrogenation experiments result in a slow diffusion of hydrogen<sup>[30]</sup> into the reaction mixture. For this reason, and for the particular case of catalyst **3**<sup>+</sup>, we must conclude that the reactions producing the hydrogenated dimer **8** and non-hydrogenated **10** become competitive. Next, we evaluated the catalytic performances of the cavplex systems in the hydrogenation of NBD under reaction and analytical conditions identical to those above (1 mol-% of **3**·BF<sub>4</sub> and 1.2 mol-% of **2a–d** at room temp. and under 1 atm H<sub>2</sub>).

The **2a**+**3**<sup>+</sup> system (Entry 4) produces norbornene (**6**) and nortricyclene (**7**) in a 3:2 ratio. This result corresponds to a moderate increase in the amount of norbornene produced relative to the model system (Entry 5). We ascribe this increase in norbornene production to a high catalytic activity of the *endo*-**2a**·Rh(NBD)<sup>+</sup> complex present in solution in low amount (<10%). At first sight, the system **2b**+**3**<sup>+</sup> seems to be less efficient in the production of norbornene than **2a**+**3**<sup>+</sup>. However, if the product distribution obtained for **2b**+**3**<sup>+</sup> is compared with that of the corresponding model systems **5b**+**3**<sup>+</sup> then the opposite conclusion is reached. As we did for the **2a**+**3**<sup>+</sup> system, we also ascribe the norbornene production for **2b**+**3**<sup>+</sup> to the *endo*-**2b**·Rh(NBD)<sup>+</sup> complex, now present in solution in larger amounts (21%). Consistently with this explanation, the system **2c**+**3**<sup>+</sup>, lacking an *endo* geometry complex assisted by N-coordination, is less effective in norbornene production.

Probably the inclusion complexes of **2c** are competent in norbornene production but they are less active than the N-coordinated counterpart **2c**·Rh(NBD)<sup>+</sup> that mainly yields nortricyclene (**7**).

Finally, the results obtained for the system **2d**+**3**<sup>+</sup> also support the competence of the inclusion complexes (NBD) Rh<sup>+</sup>·**2d** and **3**<sup>+</sup>·**2d** in the production of norbornene (**6**). However, the percentages of produced norbornene are lower than for the system **1**+**3**<sup>+</sup>. We explain this result by considering that the elimination in **2d** of one of the amide groups at the upper rim, with respect to **1**, distorts the aromatic cavity and makes its inclusion complexes with Rh(NBD)<sup>+</sup> thermodynamically less stable. In turn, the reduced thermodynamic stability of the inclusion complexes of **2d** relative to **1** translates into the presence of significant amounts of free **3**<sup>+</sup> in solution, as already observed in the binding experiment. By the same token, the release of Rh(NBD)<sup>+</sup> or **3**<sup>+</sup> into solution during hydrogenation must be favored for **2d** in relation to **1**. The low levels of nortricyclene (**7**) present in the crude products of Entries 1, 2, 3, 10, and 11 attest that the *exo* species with N coordination to the Rh<sup>I</sup> metal center must be responsible for its production.

## Conclusions

The structural modifications of cavitand **1** represented by the cavitand series **2a–c** are not successful in allowing their application as ligands for the exclusive rhodium-catalyzed hydrogenation of NBD (**4**) to norbornene (**6**). The emergence of *exo* geometries in the complexes formed between **2a–c** and **3**<sup>+</sup> provides a new reaction pathway that was not important in the case of **1**. The *exo* complexes feature a coordination bond between the nitrogen atom of the pyridyl residue at the upper rim of cavitands **2a–c** and the metal center of (NBD)Rh<sup>+</sup>. In agreement with the results obtained for the model systems **5a–c**, the *exo* coordination complexes are competent in producing nortricyclene (**7**) as the main hydrogenation product of NBD. In addition, the significant levels of norbornene (**6**) produced in the hydrogenation of NBD when the supramolecular systems **2a–d** and **3**<sup>+</sup> are employed as catalysts is attributed to a reaction pathway involving the inclusion of the Rh<sup>I</sup> metal center in the deep cavities of the hosts. In the *endo* complexes of **2a** and **2b** the cavitand may act as a first- or second-sphere ligand depending on the type of interaction established with the included rhodium center. The obtained results are not conclusive in supporting the hypothesis that *endo* complexes assisted by coordination with the pyridyl residue can also modulate the conversion of NBD into nortricyclene (**7**).

## Experimental Section

**General Methods:** All reagents and solvents were obtained from commercial suppliers and used without further purification unless otherwise stated. Cavitands **1** and **2f** were synthesized by the experimental procedure published by Rebek.<sup>[21,23]</sup> Dimer molecules **8** and **10** were synthesized by the procedure published by Katz.<sup>[22,29]</sup> 1D

and 2D NMR spectra were recorded with a Bruker Avance 400 or a Bruker Avance 500 spectrometer. All deuterated solvents (Sigma–Aldrich) were used without any further purification. Chemical shifts are given in ppm and peaks are referenced relative to the solvent residual peak ( $\delta_{\text{CH}_2\text{Cl}_2} = 5.32$  ppm,  $\delta_{\text{CHCl}_3} = 7.26$  ppm,  $\delta_{\text{DMSO}} = 2.49$  ppm). All NMR  $J$  values are given in Hz. All MS were recorded with a Bruker MALDI-TOF Autoflex instrument. Product distributions were analyzed by use of an Agilent gas chromatograph 6890N with a FID detector. Melting points were determined with a Mettler Toledo MP70 Melting Point System.

**General Procedure for the Synthesis of Cavitands 2a–d:** The nitro group in **2f** was reduced to the corresponding amine **2e** followed by acylation under Schotten–Baumann conditions to afford the desired cavitands **2a–d** in good yields after purification by column chromatography.

A typical synthetic procedure is described. A solution of **2f** (428 mg, 0.313 mmol, 1 equiv.) in THF (25 mL) was placed in a 50 mL two-necked flask. A catalytic amount of Raney-Ni (washed four times with THF, followed by separation with a magnet and decantation) was added to this solution. The mixture was stirred with a magnetic bar and purged with hydrogen (by passing hydrogen over the solution for a few seconds). The hydrogenation reaction was performed under hydrogen (1 atm) and at 40 °C for 2 h. The resulting solution was filtered through a 0.45  $\mu\text{m}$  syringe filter to remove the catalyst, and the solvent was removed under reduced pressure, affording **2e** (410 mg, 0.306 mmol, 98%).

The amino cavitand **2e** was immediately used in the next reaction step – acylation of the amine group under Schotten–Baumann conditions to produce cavitands **2a–d**. To obtain **2b**, for example, the experimental procedure consisted of adding a solution of potassium carbonate (1.2 g, 8.68 mmol, 28 equiv.) in water (18 mL) to a solution of **2e** (410 mg, 0.306 mmol, 1 equiv.) in ethyl acetate (25 mL). Next, solid nicotinoyl chloride (142 mg, 0.96 mmol, 3 equiv.) was added to the above solution in small portions with vigorous stirring. The mixture was stirred at room temperature for 16 h under nitrogen. After this time, the organic phase was separated, dried with anhydrous sodium sulfate, and filtered, and the solvent was evaporated in vacuo. The solid residue obtained was purified by flash column chromatography on silica with a gradient of methanol (0–5%) in dichloromethane to afford **2b** (390 mg, 0.27 mmol, 86%) as a solid.

By use of similar experimental procedures the cavitand **2a** was isolated in 77% yield, **2c** in 69% yield and **2d** in 79% yield.

**Cavitand 2a:** Crystals suitable for X-ray crystal structure analysis were obtained.<sup>[31]</sup> M.p. >250 °C with decomposition. <sup>1</sup>H NMR (400 MHz, [D<sub>2</sub>]dichloromethane):  $\delta = 9.79$  (s, 1 H), 9.56 (s, 1 H), 9.54 (s, 1 H), 9.13 (s, 1 H), 8.99 (s, 1 H), 8.72 (s, 1 H), 8.59 (d,  $J = 4.2$  Hz, 1 H), 8.54 (s, 1 H), 8.18 (d,  $J = 2.6$  Hz, 1 H), 8.11 (d,  $J = 7.8$  Hz, 1 H), 7.97 (s, 1 H), 7.89 (td,  $J = 7.7, 1.7$  Hz, 1 H), 7.79 (s, 1 H), 7.77 (s, 1 H), 7.75 (s, 1 H), 7.73 (s, 1 H), 7.50 (ddd,  $J = 7.6, 4.8, 1.1$  Hz, 1 H), 7.42 (s, 1 H), 7.40 (s, 1 H), 7.37 (s, 1 H), 7.36 (s, 1 H), 7.34 (s, 1 H), 7.31 (s, 1 H), 7.27 (s, 1 H), 7.25 (s, 1 H), 7.25 (s, 1 H), 7.24 (s, 1 H), 6.84 (dd,  $J = 8.7, 2.2$  Hz, 1 H), 5.75–5.57 (m, 4 H), 2.52–2.21 (m, 20 H), 1.22 (ddd,  $J = 16.2, 13.0, 7.6$  Hz, 15 H), 1.05 (td,  $J = 7.1, 4.3$  Hz, 9 H), 0.99 (td,  $J = 7.2, 3.5$  Hz, 6 H) ppm. FTIR:  $\tilde{\nu} = \nu(\text{C–N})$  1401;  $\nu(\text{Ar})$  1599, 892;  $\nu(\text{C=O})$  1662;  $\nu(\text{alkyl})$  2964, 2935, 2875;  $\nu(-\text{NH}\cdots\text{O}=\text{O})$  3261  $\text{cm}^{-1}$ . MS (MALDI, +): calcd for C<sub>84</sub>H<sub>82</sub>N<sub>8</sub>O<sub>15</sub> + H<sup>+</sup> 1443.6; found 1443.6.

**Cavitand 2b:** Crystals suitable for X-ray crystal structure analysis were obtained.<sup>[31]</sup> M.p. >250 °C with decomposition. <sup>1</sup>H NMR (400 MHz, [D<sub>2</sub>]dichloromethane):  $\delta = 9.53$  (s, 1 H), 9.41 (s, 1 H),

9.23 (s, 1 H), 9.01 (s, 1 H), 8.91 (s, 1 H), 8.76 (s, 1 H), 8.64 (dd,  $J = 4.8, 1.7$  Hz, 1 H), 8.49 (s, 1 H), 8.10 (s, 1 H), 7.78 (dt,  $J = 7.9, 1.9$  Hz, 1 H), 7.70 (s, 1 H), 7.60 (s, 1 H), 7.58 (s, 1 H), 7.56 (s, 1 H), 7.53 (s, 1 H), 7.51 (s, 2 H), 7.50 (s, 1 H), 7.36 (s, 2 H), 7.34 (s, 2 H), 7.29 (s, 2 H), 7.27 (s, 2 H), 7.27 (s, 1 H), 7.23 (s, 1 H), 5.74 (t,  $J = 8.3$  Hz, 1 H), 5.67–5.59 (m, 2 H), 5.59–5.52 (m, 1 H), 2.62–2.18 (m, 18 H), 1.70 (hept,  $J = 7.9$  Hz, 2 H), 1.37–0.89 (m, 27 H), 0.77 (t,  $J = 7.6$  Hz, 3 H) ppm. FTIR:  $\tilde{\nu} = \nu(\text{C–N})$  1403;  $\nu(\text{Ar})$  1597, 892;  $\nu(\text{C=O})$  1664;  $\nu(\text{alkyl})$  2967, 2934, 2872;  $\nu(-\text{NH}\cdots\text{O}=\text{O})$  3251  $\text{cm}^{-1}$ . MS (MALDI, +): calcd for C<sub>84</sub>H<sub>82</sub>N<sub>8</sub>O<sub>15</sub> + H<sup>+</sup> 1443.6; found 1443.6.

**Cavitand 2c:** M.p. >250 °C with decomposition. <sup>1</sup>H NMR (500 MHz, [D<sub>2</sub>]dichloromethane):  $\delta = 9.59$  (s, 1 H), 9.45 (s, 1 H), 9.32 (s, 1 H), 8.98 (s, 1 H), 8.77–8.72 (m, 1 H), 8.61–8.55 (m, 2 H), 8.14 (s, 1 H), 7.85–7.81 (m, 1 H), 7.71 (s, 1 H), 7.58 (s, 1 H), 7.56 (s, 1 H), 7.55 (s, 1 H), 7.54 (s, 1 H), 7.52 (s, 1 H), 7.50 (s, 1 H), 7.37 (s, 1 H), 7.35 (s, 2 H), 7.34 (s, 1 H), 7.32 (s, 1 H), 7.30 (s, 1 H), 7.29 (s, 1 H), 7.28 (s, 1 H), 7.27 (s, 1 H), 7.24 (s, 2 H), 7.23 (s, 1 H), 5.73 (t,  $J = 8.4$  Hz, 1 H), 5.63 (dt,  $J = 12.5, 8.3$  Hz, 2 H), 5.57 (t,  $J = 8.3$  Hz, 1 H), 2.59–2.20 (m, 20 H), 1.33–1.17 (m, 18 H), 1.11–1.03 (m, 3 H), 1.04–0.95 (m, 6 H), 0.77 (t,  $J = 7.6$  Hz, 3 H) ppm. FTIR:  $\tilde{\nu} = \nu(\text{C–N})$  1401;  $\nu(\text{Ar})$  1599, 892;  $\nu(\text{C=O})$  1658;  $\nu(\text{alkyl})$  2963, 2935, 2874;  $\nu(-\text{NH}\cdots\text{O}=\text{O})$  3253  $\text{cm}^{-1}$ . MS (MALDI, +): calcd for C<sub>84</sub>H<sub>82</sub>N<sub>8</sub>O<sub>15</sub> + H<sup>+</sup> 1443.6; found 1443.6.

**Cavitand 2d:** Crystals suitable for X-ray crystal structure analysis were obtained.<sup>[31]</sup> M.p. >250 °C with decomposition. <sup>1</sup>H NMR (400 MHz, [D<sub>2</sub>]dichloromethane):  $\delta = 9.43$  (s, 1 H), 9.38 (s, 1 H), 9.35 (s, 1 H), 9.11 (s, 1 H), 8.36 (s, 1 H), 8.05 (dd,  $J = 8.3, 1.2$  Hz, 1 H), 7.92 (s, 1 H), 7.73 (s, 1 H), 7.63 (s, 1 H), 7.62 (s, 1 H), 7.60 (s, 1 H), 7.57 (s, 1 H), 7.50 (s, 1 H), 7.48 (s, 1 H), 7.47 (s, 2 H), 7.45 (s, 2 H), 7.43 (s, 1 H), 7.37 (s, 1 H), 7.37 (s, 1 H), 7.36 (s, 1 H), 7.35 (s, 2 H), 7.34 (s, 2 H), 7.28 (s, 1 H), 7.27 (s, 1 H), 7.25 (s, 1 H), 5.72 (t,  $J = 8.3$  Hz, 1 H), 5.68–5.59 (m, 2 H), 5.64–5.53 (m, 1 H), 2.55–2.18 (m, 16 H), 1.86–1.57 (m, 4 H), 1.31–1.16 (m, 12 H), 1.04 (ddq,  $J = 30.3, 15.6, 7.5$  Hz, 15 H), 0.76 (t,  $J = 7.5$  Hz, 3 H) ppm. FTIR:  $\tilde{\nu} = \nu(\text{C–N})$  1402;  $\nu(\text{Ar})$  1598, 892;  $\nu(\text{C=O})$  1664;  $\nu(\text{alkyl})$  2965, 2933, 2872;  $\nu(-\text{NH}\cdots\text{O}=\text{O})$  3249  $\text{cm}^{-1}$ . MS (MALDI, +): calcd for C<sub>84</sub>H<sub>82</sub>N<sub>8</sub>O<sub>15</sub> + Na<sup>+</sup> 1464.6; found 1464.6.

**General Procedure for the Synthesis of Reference Ligands 5a–d:** Under Schotten–Baumann conditions analogous to those described for the synthesis of cavitands **2a–d**, aniline was acylated to produce reference ligands **5a–d**. Crystallization from water/acetone mixtures afforded the pure compounds, in 75% yield for **5a**, 64% yield for **5b**, 43% yield for **5c**, and 89% yield for **5d**.

**N-Phenylpyridine-2-carboxamide (5a):** <sup>1</sup>H NMR (500 MHz, CDCl<sub>3</sub>):  $\delta = 10.03$  (s, 1 H), 8.62 (ddd,  $J = 4.7, 1.6, 0.9$  Hz, 1 H), 8.31 (dt,  $J = 7.8, 1.0$  Hz, 1 H), 7.91 (td,  $J = 7.7, 1.7$  Hz, 1 H), 7.79 (dt,  $J = 8.7, 1.6$  Hz, 2 H), 7.49 (ddd,  $J = 7.6, 4.8, 1.2$  Hz, 1 H), 7.43–7.33 (m, 2 H), 7.19–7.10 (m, 1 H) ppm.<sup>[32]</sup>

**N-Phenylpyridine-3-carboxamide (5b):** <sup>1</sup>H NMR (500 MHz, CDCl<sub>3</sub>):  $\delta = 9.08$  (d,  $J = 1.8$  Hz, 1 H), 8.76 (dd,  $J = 4.8, 1.6$  Hz, 1 H), 8.20 (dt,  $J = 7.9, 2.0$  Hz, 1 H), 8.04 (s, 1 H), 7.64 (d,  $J = 7.8$  Hz, 2 H), 7.43 (ddd,  $J = 7.9, 4.8, 0.8$  Hz, 1 H), 7.41–7.35 (m, 2 H), 7.21–7.16 (m, 1 H) ppm.<sup>[33]</sup>

**N-Phenylpyridine-4-carboxamide (5c):** <sup>1</sup>H NMR (500 MHz, [D<sub>6</sub>]DMSO):  $\delta = 10.48$  (s, 1 H), 9.06–8.56 (m, 2 H), 7.97–7.79 (m, 2 H), 7.76 (d,  $J = 7.7$  Hz, 2 H), 7.37 (t,  $J = 7.9$  Hz, 2 H), 7.13 (t,  $J = 7.4$  Hz, 1 H) ppm.<sup>[34]</sup>

**N-Phenylbenzamide (5d):** <sup>1</sup>H NMR (500 MHz, CDCl<sub>3</sub>):  $\delta = 7.88$  (s, 1 H), 7.86 (d,  $J = 1.5$  Hz, 2 H), 7.65 (d,  $J = 7.8$  Hz, 2 H), 7.59–

7.51 (m, 1 H), 7.48 (t,  $J = 7.5$  Hz, 2 H), 7.41–7.34 (m, 2 H), 7.16 (t,  $J = 7.4$  Hz, 1 H) ppm.<sup>[32]</sup>

**Catalytic Hydrogenation Reactions:** A typical laboratory-scale hydrogenation experiment consisted of dissolving **3**·BF<sub>4</sub> (20 μmol) and the appropriate cavitand or model ligand (**1**, **2a–d**, **5a–d**, 25 μmol) in dichloromethane (HPLC grade, 6.8 mL). The resulting solution was transferred to a 25 mL three-necked flask fitted with a hydrogen inlet. The catalyst was preactivated by purging the flask with hydrogen and stirring the mixture under 1 bar of hydrogen for 5 min. Next, neat norbornadiene (**4**, 2.12 mmol) was added in one shot, and the reaction evolution was immediately sampled by taking small aliquots of the reaction mixture (100 μL). Aliquots were taken every 15 min. Each aliquot was diluted with dichloromethane (100 μL), filtered through a silica gel plug, and analyzed by GC/FID.

**Supporting Information** (see footnote on the first page of this article): <sup>1</sup>H NMR spectra and MALDI-MS isotopic distributions for synthesized cavitands, 2D <sup>1</sup>H NMR spectra of the encapsulation complexes, <sup>1</sup>H NMR spectra for competitive titration studies, GC/FID traces for catalytic experiments.

## Acknowledgments

The authors are grateful for funding from the Ministerio de Economía y Competitividad (MINECO) (CTQ2011-23014), the Generalitat de Catalunya DIUE (2009SGR6868), and the ICIQ Foundation.

- [1] P. W. N. M. van Leeuwen (Ed.), *Supramolecular Catalysis*, 1st ed., Wiley-VCH, Weinheim, Germany, 2008.
- [2] M. Raynal, P. Ballester, A. Vidal-Ferran, P. W. N. M. van Leeuwen, *Chem. Soc. Rev.* **2014**, *43*, 1660–1733.
- [3] M. Raynal, P. Ballester, A. Vidal-Ferran, P. W. N. M. van Leeuwen, *Chem. Soc. Rev.* **2014**, *43*, 1734–1787.
- [4] A. Cavarzan, J. N. H. Reek, F. Trentin, A. Scarso, G. Strukul, *Catal. Sci. Technol.* **2013**, *3*, 2898–2901.
- [5] B. W. Purse, A. Gissot, J. Rebek, *J. Am. Chem. Soc.* **2005**, *127*, 11222–11223.
- [6] T. Murase, Y. Nishijima, M. Fujita, *J. Am. Chem. Soc.* **2012**, *134*, 162–164.
- [7] C. J. Hastings, M. P. Backlund, R. G. Bergman, K. N. Raymond, *Angew. Chem. Int. Ed.* **2011**, *50*, 10570–10573; *Angew. Chem.* **2011**, *123*, 10758.
- [8] J. Meeuwissen, J. N. H. Reek, *Nature Chem.* **2010**, *2*, 615–621.
- [9] H. J. Hwang, J. R. Carey, E. T. Brower, A. J. Gengenbach, J. A. Abramite, Y. Lu, *J. Am. Chem. Soc.* **2005**, *127*, 15356–15357.
- [10] T. S. Koblenz, J. Wassenaar, J. N. H. Reek, *Chem. Soc. Rev.* **2008**, *37*, 247–262.
- [11] M. A. Sarmentero, H. Fernández-Pérez, E. Zuidema, C. Bo, A. Vidal-Ferran, P. Ballester, *Angew. Chem. Int. Ed.* **2010**, *49*, 7489–7492; *Angew. Chem.* **2010**, *122*, 7651.
- [12] D. Fiedler, R. G. Bergman, K. N. Raymond, *Angew. Chem. Int. Ed.* **2006**, *45*, 745–748; *Angew. Chem.* **2006**, *118*, 759.
- [13] Z. J. Wang, C. J. Brown, R. G. Bergman, K. N. Raymond, F. D. Toste, *J. Am. Chem. Soc.* **2011**, *133*, 7358–7360.
- [14] A. Cavarzan, A. Scarso, P. Sgarbossa, G. Strukul, J. N. H. Reek, *J. Am. Chem. Soc.* **2011**, *133*, 2848–2851.
- [15] V. F. Slagt, J. N. H. Reek, P. C. J. Kamer, P. W. N. M. van Leeuwen, *Angew. Chem. Int. Ed.* **2001**, *40*, 4271–4274; *Angew. Chem.* **2001**, *113*, 4401.
- [16] A. W. Kleij, J. N. H. Reek, *Chem. Eur. J.* **2006**, *12*, 4219–4227.
- [17] V. F. Slagt, P. C. J. Kamer, P. W. N. M. van Leeuwen, J. N. H. Reek, *J. Am. Chem. Soc.* **2004**, *126*, 1526–1536.
- [18] B. Kang, J. W. Kurutz, K. T. Youm, R. K. Totten, J. T. Hupp, S. T. Nguyen, *Chem. Sci.* **2012**, *3*, 1938–1944.
- [19] C. J. Brown, G. M. Miller, M. W. Johnson, R. G. Bergman, K. N. Raymond, *J. Am. Chem. Soc.* **2011**, *133*, 11964–11966.
- [20] D. M. Rudkevich, G. Hilmersson, J. Rebek, *J. Am. Chem. Soc.* **1997**, *119*, 9911–9912.
- [21] D. M. Rudkevich, G. Hilmersson, J. Rebek, *J. Am. Chem. Soc.* **1998**, *120*, 12216–12225.
- [22] R. J. Roth, T. J. Katz, *Tetrahedron Lett.* **1972**, *13*, 2503–2504.
- [23] O. B. Berryman, A. C. Sather, A. Lledó, J. Rebek, *Angew. Chem. Int. Ed.* **2011**, *50*, 9400–9403; *Angew. Chem.* **2011**, *123*, 9572.
- [24] A. Szumna, *Chem. Soc. Rev.* **2010**, *39*, 4274–4285.
- [25] The stereochemical designations are described in the following sequence: axial chirality (*P* or *M*), defined by the unidirectional (clockwise or counterclockwise) sense of rotation of the seven amide carbonyl groups viewed from above the cavity, followed by the absolute configuration, by application of the CIP rules, of the methyne (*R* or *S*) in the nine-membered ring containing the asymmetric phenyldioxo bridge.
- [26] J. R. Moran, J. L. Ericson, E. Dalcanale, J. A. Bryant, C. B. Knobler, D. J. Cram, *J. Am. Chem. Soc.* **1991**, *113*, 5707–5714.
- [27] A. J. Pardey, C. Longo, *Coord. Chem. Rev.* **2010**, *254*, 254–272.
- [28] A. Hamilton, M. Gicquel, P. Ballester, C. Bo, *Curr. Org. Chem.* **2013**, *17*, 1499–1506.
- [29] J. J. Mrowca, T. J. Katz, *J. Am. Chem. Soc.* **1966**, *88*, 4012–4015.
- [30] M. B. Krüger, C. Selle, D. Heller, W. Baumann, *J. Chem. Eng. Data* **2012**, *57*, 1737–1744.
- [31] CCDC-990079 (for **2a**), -990080 (for **2b**), and -990081 (for **2d**) contain the supplementary crystallographic data for this paper. These data can be obtained free of charge from The Cambridge Crystallographic Data Centre via [www.ccdc.cam.ac.uk/data\\_request/cif](http://www.ccdc.cam.ac.uk/data_request/cif).
- [32] L. Zhang, W. Wang, A. Wang, Y. Cui, X. Yang, Y. Huang, X. Liu, W. Liu, J.-Y. Son, H. Oji, T. Zhang, *Green Chem.* **2013**, *15*, 2680–2684.
- [33] W. Fang, Q. Deng, M. Xu, T. Tu, *Org. Lett.* **2013**, *15*, 3678–3681.
- [34] K. Motoshima, Y. Hiwasa, M. Yoshikawa, K. Fujimoto, A. Tai, H. Kakuta, K. Sasaki, *ChemMedChem* **2007**, *2*, 1527–1532.

Received: April 10, 2014  
Published Online: June 3, 2014